A conceptual design and feasibility study of a lithium–air battery electric narrowbody aircraft with 700 nm range

Gregory Northwood, and Jenny Baker
Faculty of Science and Engineering, University of Bath, Claverton Down, Bath, United Kingdom, BA2 7AY

This work investigates the feasibility of a fully electric narrowbody commercial aircraft based on the Airbus A320 platform. The study adopts solid-state lithium–air batteries at 1,150 Wh/kg. A conventional tube-and-wing configuration with eight spanwise-distributed electric propulsors is developed through an iterative sizing convergence loop coupling the constraint diagram, mass build-up, wing geometry, and mission simulation. Sensitivity analyses are conducted across wingspan, cruise altitude, cruise Mach number, and battery energy density. The optimised design converges to a 52 m wingspan (ICAO Code D), an initial cruise altitude of 25,000 ft, and a cruise Mach number of 0.5. At these conditions, the 700 nm design range, is achieved with a maximum take-off weight of 88.8 tonnes, a battery and oxygen system mass of 29.0 tonnes, and a positive remaining cargo volume of 35.3 m^3. The manufacturing carbon deficit relative to a conventional A320 propulsion system is recovered within approximately 104 flights against the A320neo under a near-renewable charging grid, roughly two weeks of typical utilisation. Against the world average 2025 grid, break-even is 196 flights, approximately one month of operation. Over a 20-year service life, the aircraft cuts lifetime CO_2 emissions by 93 % against the A320neo on a near-renewable grid. The electric aircraft is cheaper per flight at all historically observed jet fuel prices, achieving a 25% reduction in direct operating cost and a 15 % reduction in 20-year total cost of ownership at baseline assumptions. Whilst there are still significant barriers such as safety and battery technology readiness this work highlights the potential of electric flight to achieve improvements in both environmental impact and flight cost compared with current aircraft.

Nomenclature

APU	=	Auxillary power unit
AR	=	Aspect ratio
A320neo	=	A320 new engine option
A320ceo	=	A320 current engine option
CD0	=	Zero life drag coefficient
CFRP	=	Carbon fibre reinforced polymer
C-rate	=	Charge rate of the battery
C_{Lmax}	=	Maximum lift coefficient
DOC	=	Direct operating cost
e	=	Oswald efficiency
EGT	=	Exhaust gas temperature
EFH	=	Engine flight hour
fW	=	Weight factor
fS	=	Scale factor
hsc	=	Screen height
ICA	=	Initial cruise altitude
LCA	=	Life cycle assessment
L/D	=	Lift to drag ratio
LOX	=	Liquid oxygen
K	=	Induced drag factor
m	=	Mass
M	=	Cruise Mach number
MLW	=	Maximum landing weight
MRO	=	Maintenance, repair and overhaul
MTOW	=	Maximum take of weight
MZFW	=	Maximum zero fuel weight
OEW	=	Operating empty weight
PMSM	=	Permanent – magnet synchronous machines

P/W	=	Power to weight ratio
S_{TO}	=	Take off field length
S land	=	Landing field length
SiC	=	Silicon carbide
W/S	=	Wing loading
V_{app}	=	Approach speed
γ_{climb}	=	Take of climb angle
η_{prop}	=	Propeller efficiency
σ	=	Altitude
ψ	=	Bending relief parameter

I.Introduction

Aviation faces increasing pressure to reduce its environmental impact, contributing approximately 3.5% of global CO_2 emissions in 2011, and whilst there is uncertainty associated with the impact of non CO_2 forcing this is estimated to be three times that of CO_2 emissions alone[1]. Demand for air travel continues to grow[2] particularly in the short-haul sector, making meaningful emissions reduction both urgent and challenging. By eliminating in-flight combustion, electric aircraft can significantly reduce lifecycle emissions, particularly when powered by low-carbon electricity. In addition, higher propulsive efficiency and reduced mechanical complexity offer the prospect of lower operating costs, presenting both an environmental and economic opportunity. Recent advances in battery and electric motor technology, driven largely by the automotive sector, have improved energy density, reduced cost, and increased power capability[3]. These developments make it timely to reassess the feasibility of electric propulsion for transport aircraft.

State-of-the-art lithium-ion cells based on high-nickel cathodes and graphite anodes achieve 250–300 Wh/kg at cell level [4,5]. Emerging variants incorporating silicon-composite anodes and single-crystal cathodes are projected to reach 350–400 Wh/kg by the late 2020s[6,7]. However, fundamental intercalation limits constrain graphite anodes to a theoretical capacity of 372 mAh/g, and cathode structural stability degrades at higher nickel content, establishing an effective ceiling for conventional lithium-ion architectures[5]. At these energy densities the battery mass required to match even a fraction of the conventional fuel energy exceeds the structural capacity of the airframe. Achieving practical electric flight on a commercial scale therefore requires a step change in energy density beyond what current lithium chemistries can deliver. Lithium–sulphur batteries (Li–S) offer a theoretical specific energy of approximately 2,600 Wh/kg at the reaction level, arising from the high capacity of the sulphur cathode and the use of lithium metal as the anode[8,9]. Practical cell-level demonstrations in pouch-cell formats have reached 300–450 Wh/kg, with 410 Wh/kg cells used to power the KARI EAV-3 high-altitude drone [4]. However, Li–S systems face challenges that limit their suitability for aviation: polysulphide shuttling causes progressive capacity fade, volumetric expansion of the sulphur cathode induces mechanical degradation, and cycle life remains limited to 60–200 cycles in high-energy configurations[4,5]. Li–S technology is therefore better suited to low-cycle, weight-critical applications such as high-altitude pseudo-satellites than to commercial aircraft requiring high numbers of cycles.

Lithium–air ($Li–O_2$) batteries offer the highest theoretical specific energy of any rechargeable electrochemical system, with values of 3,460–3,505 Wh/kg when oxygen mass is excluded[8,9]. However, conventional liquid-electrolyte Li–air systems suffer from fundamental limitations, including electrolyte instability, cathode passivation, high overpotentials, and lithium dendrite formation[8,10,11]. As a result, no system has demonstrated aviation-relevant cycle life or durability. Solid-state lithium–air batteries address many of these issues by replacing the liquid electrolyte with a solid ion conductor, improving safety and reducing parasitic reactions[12]. Kondori et al[13] demonstrate capacities of 685 Wh/kg under 1C deep discharge, alongside round-trip efficiencies of > 90 % which are maintained at > 87 % after 1000 cycles. Solid Energies [14] have reported specific energies density of 1,150 Wh/kg at low C rate (C/5) with a road map to achieving this capacity at a power of 500W/kg in larger format cells, supporting the future feasibility of the 1,150 Wh/kg adopted in this study. Wang et al.[15] demonstrated that wing-integrated batteries substantially reduce optimised wing mass compared to fuselage-housed configurations whilst Karadotcheva et al. [16] identified the wing as the most promising location for multifunctional energy storage integration, particularly on the lower panels where tension dominates.

After batteries, electric propulsion is a key enabler with development of multi-megawatt electric propulsion driven by both aerospace and adjacent industrial applications. The Rolls-Royce ACCEL programme achieved first flight of the Spirit of Innovation in September 2021 using a 400 kW permanent-magnet machine with an integrated SiC inverter, subsequently setting a world electric-aircraft speed record of 555.9 km/h[17]. H3X Technologies has claimed 13–15 kW/kg continuous at the bare-motor level for its HPDM-250 integrated motor, with motor-only specific power values are approaching or exceeding 10 kW/kg, but installed powertrain values remain around 5–7 kW/kg to added mass from inverter, cooling, and mounting hardware[18,19]. A historical assessment fitted growth curves to industrial and aerospace machine data[20], projects a 2030 nominal specific power of 13.2 kW/kg, with conservative and aggressive bounds of 9.2 and 16.1 kW/kg respectively, including thermal management systems. Electric motors achieve peak efficiencies of 95–97 % across a broad operating envelope, compared to approximately 35–40 % for turbofans at cruise and significantly lower values on-load [21]. They are mechanically simpler, with orders of magnitude fewer components and no combustion system reducing maintenance complexity and improving reliability[22,23]. For the lower cruise speeds and altitudes characteristic of battery-electric aircraft, propeller-based propulsion offers higher propulsive efficiency than turbofans, as efficiency scales with disc area rather than exhaust jet velocity[24,25]. Electric motors also provide high torque at low rotational speeds, enabling effective thrust control and reverse thrust via propeller pitch or direction reversal without the wear constraints associated with turbofan systems[23,26]. Electric propulsion produces no local emissions and operates at significantly lower noise levels, offering advantages for airport operations subject to stringent environmental and acoustic constraints [27]. Spanwise-distributed electric propulsors provide two categories of benefit beyond thrust generation: aerodynamic lift augmentation and relaxation of empennage sizing requirements[27]. Propeller slipstreams increase local dynamic pressure, delaying separation and enhancing flap effectiveness [27–29]. Studies report maximum lift coefficient (C_{Lmax}) increases ranging from 10–30% for aircraft, with higher values achievable under strong blowing conditions[28,30,31].

This study adopts a pure-electric propulsion architecture to directly address the research question of whether electric flight is feasible for an A320-class mission. The pure-electric case represents the most stringent constraint, defining the limits of battery-based flight capability. From an environmental perspective, pure-electric propulsion uniquely eliminates in-flight CO_2 and non-CO_2 climate impacts, including contrails and NOx-induced effects[1]. The design space at intermediate battery specific energies (~1,150 Wh/kg) remains relatively underexplored. Much of the literature instead focuses either on battery specific energies of approximately 350-750 Wh/kg[32,33], where electric transport aircraft are generally found to be severely range- or payload-limited, or on studies assuming battery specific energies exceeding ~1,000 Wh/kg as enabling technologies for larger commercial aircraft[34].

The intermediate regime utilizing lithium-O_2 batteries[35], where feasibility is marginal, provides the most insight into system-level trade-offs and defines the contribution of this work. To the best of the authors knowledge this is the first study to compare the impacts of oxygen supply from LOX stored onboard with oxygen compressed and separated from the atmosphere during flight. We evaluate technical feasibility, environmental performance, and commercial viability to determine whether electric flight can become a practical alternative to conventional aviation.

II.Methodology

This work adopts a conventional tube-and-wing configuration representative of the A320 class, leveraging the maturity of established transport-aircraft architectures in aerodynamic behaviour, structural load paths, system integration, and certification [24]. While blended wing body configurations offer potential gains in aerodynamic efficiency and internal volume, their development complexity and immature certification pathways are misaligned with a near-term entry-into-service objective [36]. The conventional configuration also enables direct comparison with the A320 in terms of capacity, airport compatibility, and mission profile, supporting a realistic assessment of electrification feasibility within the narrowbody segment. This work combines the four technology domains into a single integrated concept. Solid-state lithium–air cells at 1,150 Wh/kg with onboard liquid oxygen storage provide the energy system, driving eight distributed permanent-magnet synchronous machines at 13.2 kW/kg whose augmentation enables higher wing loading and reduced empennage sizing. A full transition to CFRP construction offsets the increased energy-system weight[37], an aircraft schematic is given in Figure 1a.

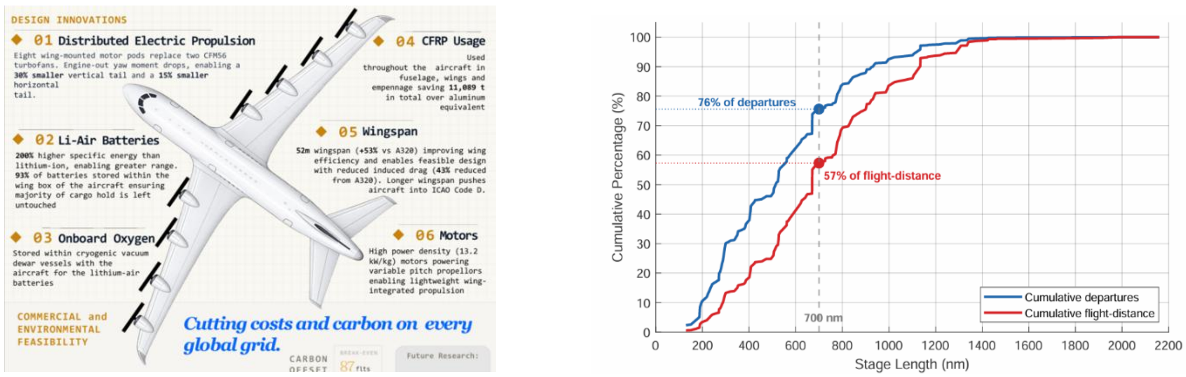

Figure 1 (a) – Schematic of aircraft with distributed propulsion and battery and LOX locations, (b) Cumulative coverage of A320 departures from London Heathrow by great-circle distance

The design objective is not to replicate the maximum range capability of the conventional platform, but rather to achieve competitiveness across the stage lengths that account for the largest proportion of real-world operations. To quantify this requirement, operational flight data for 2023 A320 services were analysed for departures from Birmingham Airport and Heathrow Airport, representing a major regional hub and a primary international hub respectively. Stage-length distributions[38] indicate that a design range of 700 nautical miles would enable the electric aircraft to perform: 88% and 76 % of A320 departures from Birmingham and Heathrow respectively, corresponding to 68% and 57% of flight distance, Figure 1b. To maintain commercial equivalence with the Airbus A320 class, passenger capacity (150 persons) requirements are preserved by adopting fuselage dimensions consistent with the baseline A320 platform. This approach provides several key advantages: direct comparison against an established narrowbody transport standard; preservation of airport interface compatibility (gate geometry, jet bridges, ground handling equipment); and realistic payload assumptions for mission sizing and constraint analysis. Passenger and cargo payload masses are retained at baseline A320 values, Table 1, although the cargo volume available for freight was not fixed.

Parameter	Value
Aircraft Variant	Airbus A320-200
Typical Seating Capacity	150 passengers
Range	6,300 km
Wingspan (with sharklets)	35.8 m
Wing Area	122.6 m^2
Maximum Take-Off Weight (MTOW)	78,000 kg
Maximum Landing Weight (MLW)	66,000 kg
Operating Empty Weight (OEW)	42,000–44,000 kg
Maximum Fuel Capacity	15,842 L
Engines	2 × CFM56-5B (typical)
Maximum Thrust (per engine)	120 kN
Cruise Mach Number	0.78

Table 1: Key characteristics of the Airbus A320-200

Lithium-air batteries achieve high theoretical specific energy by using oxygen as the cathode reactant, during discharge, lithium metal reacts with oxygen to form lithium peroxide the key battery and oxygen system parameters are summarised in Table 2.

Parameter	Value
Electrical energy yield per kg O_2 (supporting info Eqn 8.1)	9.72 kWh / kgO_2
Useable depth of discharge	80 %
System margin	10%
Cell – level volumetric energy density	950 Wh/l
Volumeteric packing density	0.65
LOX density	1141 kg/m^3
Dewar packing factor	0.8

Table 2: Oxygen system parameters for lithium- air battery

A conservative usable discharge fraction of 80% is adopted to preserve cycle life and maintain reversible electro chemistry[8]. Combined with the 10% system margin, 88% of the theoretical oxygen capacity is filled during each mission. A full safety case for onboard LOX, including containment, venting, crash survivability, and ground handling protocols, is beyond the scope of this conceptual design study but is identified as a critical area for further investigation. The initial concept design assumes onboard LOX storage in a vacuum-insulated composite vessel with a metallic liner and is compared with an alternative architecture that uses atmospheric oxygen as the cathode reactant should onboard oxygen storage prove impractical. For context, the baseline Airbus A320 crew oxygen system carries approximately 4.7 kg of oxygen[39].

III.Preliminary Design

By replacing the conventional fuel mass at 700 nm, with the scaled battery mass and maintaining the existing structural baseline, a preliminary electric MTOW of approximately 108 t was estimated representing an increase of ~ 37% compared to the conventional aircraft, Table 3.

Parameter	Value
Total fuel chemical energy (full range)	548,765 MJ
Equivalent battery mass (full range, 1150 Wh/kg)	132.5 t
Target range	700 nm
Battery mass (700 nm, first-order estimate)	23.5 t
Preliminary electric MTOW	≈ 108 t
MTOW increase vs. conventional A320	≈ 37%

Table 3: Preliminary electric conversion estimates.

Two modifications to the baseline A320 drag polar are applied at the preliminary design stage. First, the A320neo Sharklet wingtip devices increase the effective aspect ratio and improve span efficiency, reducing induced drag. A conservative 10% reduction in the induced drag factor is adopted, applied solely through the induced drag term with the zero-lift drag coefficient unchanged at this stage. Second, the aerodynamic implications of replacing the twin turbofan installation with eight distributed electric propulsors were assessed using a conventional parasite drag build-up method and an Oswald efficiency formulation (supporting information page 2-3). The analysis considered changes in zero-lift drag from nacelle and pylon removal, addition of distributed propulsor pods, and modification of the Oswald efficiency factor. The net change in zero-lift drag is small and lies within the uncertainty bounds of conceptual wetted-area estimation.

The constraint diagram, Figure 2, defines the feasible design space in terms of wing loading (W/S) and power-to-weight ratio (P/W) [40]. Each performance requirement imposes a boundary, with the feasible region lying above power constraints and below wing-loading limits. The design point is selected at maximum wing loading and minimum power-to-weight ratio to minimise structural and propulsion mass. Constraint relations are applied within the convergence loop, using the current MTOW to determine wing area and installed power at each iteration. All constraints are based on A320 operational requirements[41], with adjustments for electric propulsion. The cruise condition of 32,000 ft at Mach 0.7 reflects the upper operating envelope of modern turbo prop aircraft, such as the Airbus A400M [42]. A weight factor (fW) , of 1.02 is applied throughout to account for maneuver and gust load increases during size, and a scale factor (fS) of 0.985 corrects for differences between the maximum lift coefficients demonstrated and certified [43]. Five operational constraints are evaluated in the constraint diagram, each imposing a boundary in the wing loading–power loading design space. The initial cruise altitude (ICA) constraint requires the aircraft to maintain steady level flight at the design cruise Mach number at the target cruise altitude. A cruise power setting of 90 % of installed power is assumed, the climb with 20 % power inoperative constraint ensures that the aircraft can maintain the CS-25[44] minimum second-segment climb gradient of 2.4 % with one-fifth of the installed power unavailable, equivalent to losing approximately two of the eight distributed motors [45]. The take-off field length constraint requires the aircraft to become airborne, clear a 35 ft screen height, and climb away within 2180 m. The approach speed constraint imposes a maximum wing loading to ensure the certified approach speed of 140 kt can be maintained with the landing configuration deployed, this appears as a vertical line on the constraint diagram, Figure 2.

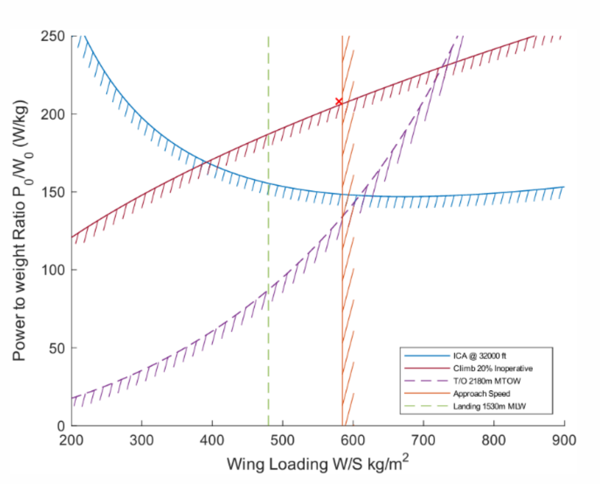

Parameter	Description	Value
S_{TO}	Take-off field length (MTOW, ISA, SL)	2180 m
S_{land}	Landing field length (MLW)	1530 m
V_{app}	Approach speed	140 kt
$C_{L,\mathrm{max,land}}$	Max lift coefficient, landing config.	$3 \times 1.15 = 3.4$
$C_{L,\mathrm{max,TO}}$	Max lift coefficient, take-off config.	$2.56 \times 1.3 = 3.3$
h_{ICA}	Initial cruise altitude	32,000 ft
M_{ICA}	Cruise Mach number (ICA)	0.7
γ_{climb}	Take-off climb angle	10°
h_{sc}	Screen height (CS-25)	35 ft
η_{prop}	Propeller efficiency (altitude-dependent)	$0.92 \times \sigma^{0.05}$

Figure 2 (a) Preliminary constraint diagram (b) model input parameters, derived from A320 requirements.

The landing field length constraint provides an independent maximum wing loading from the certified landing distance of 1530 m. For an electric aircraft, the landing-to-take-off mass ratio is close to 1 since no fuel and only oxygen is burned, which tightens this constraint relative to conventional aircraft. Full expressions for each constraint, including propeller efficiency, power lapse, and atmospheric density corrections, are given in the supporting information page 6. The design point is selected at the maximum wing loading and minimum power-to-weight ratio, with margins of 3 W/kg and 5 kg/m^2 for operational flexibility. Maximising wing loading reduces wing area, lowering structural mass and drag. Wing area and installed power are updated iteratively with MTOW. The landing field length constraint is included but not active. Under CS-25[44] reverse thrust is not credited in landing distance calculations for turbofan aircraft due to reliability and wear considerations[26,40]. In contrast, electric motors can provide reliable reverse thrust through rapid reversal of propeller rotation, analogous to certified reverse-pitch turboprop systems[46] allowing the landing constraint to be relaxed, and the approach speed constraint remains the governing limit on wing loading.

The constraint diagram design point, combined with the preliminary MTOW estimate from Table 3, yields a first set of sizing parameters for the electric derivative, Table 4.

Parameter	A320-200	Preliminary Electric	Δ
Mass and Loading			
MTOW (t)	78.0	~108	+38%
MZFW (t)	60.5	~65	+7%
Energy carrier mass (t)*	12.7	~40.8	—
Payload (t)	19.15	19.15	0
Geometry			
Wingspan (m)	35.8	35.8 (Code C)	0
Wing area (m^2)	122.6	~183	+49%
Aspect ratio	10.3	~7.0	−32%
Wing loading (kg/m^2)	636	~590	−7%
Propulsion			
Installed power/thrust	2x120 kN	22.7 MW	—
Mission			
Design range (nm)	3 400	700	−79%
Cruise altitude (ft)	37 000	32 000	−14%
Cruise Mach	0.78	0.70	−10%

Table 4: Preliminary comparison of the electric derivative against the A320-200 baseline.

Three observations from Table 4 motivate the iterative design process; first, the MTOW of ~108t is a 38% increase over the conventional A320 and is likely to violate the available wing box volume, since the energy carrier mass has more than tripled while the wing dimensions are held fixed. To recover cargo volume the wingspan must grow beyond the Code C limit to Code D (52 m max wingspan). Second, the preliminary wing area of 183 m^2 is substantially larger than the A320's 122.6 m^2, driven by the lower cruise altitude and Mach needed to reach the ICA constraint at acceptable power loadings; this compounds the wing mass penalty and couples back into MTOW through the convergence loop. Third, the installed power loading of 210 W/kg is dictated by the constraint diagram rather than by a free choice and will evolve as the cruise Mach and altitude are revised in the sensitivity analyses.

IV.Iterative Design Results

The aircraft is sized through a coupled convergence loop in which the physical dimensions, structural masses, and energy requirements are updated iteratively until a consistent design is reached, within the Code D limit. An initial MTOW estimate is formed from the preliminary design process previously discussed. This estimate enters the constraint diagram, where the wing loading and power-to-weight ratio are determined. Because the induced drag factor depends on the aspect ratio, which in turn depends on the wing area, the constraint diagram is re-evaluated at every iteration. With $W/S$and P_0/W_0 defined, the current MTOW determines the wing area, installed power, motor mass, and aspect ratio.

The wing design step computes the available internal volume for battery storage using the real aerofoil geometry, and determines how much battery mass can be accommodated within the wing box, and evaluates the bending relief parameter (ψ) and the corresponding wing structural mass. The mission simulation then models the 700 nm profile plus the reserves. The required battery hardware and liquid oxygen mass are calculated, together forming the updated energy system mass, ($m_{\text{batt,new}}$). This battery mass is allocated first to the outboard wings, then to the centre wing box, and finally to the fuselage cargo holds, with a volume feasibility check performed at each stage. The updated MTOW is then computed. If the change from the previous iteration satisfies eqn 1.

$$| m_{TO,\text{new}} - m_{TO,\text{old}} | < 10 \text{ kg}, \qquad \text{Eqn 1}$$

the design is considered converged; otherwise, the updated MTOW is fed back into the constraint diagram and the loop is repeated. Convergence is typically achieved within 8-12 iterations.

A. Drag Calculations

The baseline A320 zero-lift drag coefficient CD0 = 0.018 includes contributions from all major airframe com ponents. Replacing the twin turbofan installation with eight distributed electric motors, and exploiting the yaw-control redundancy of distributed propulsion to reduce empennage area, produces three independent modifications to the zero-lift drag. Each is evaluated below using the Raymer component build-up method[40]. The A320 installation comprises two CFM56 turbofan nacelles (each 2.7 m diameter × 5.1 m length) mounted on wing pylons, using the Raymer nacelle form factor and an interference factor for a pylon-mounted nacelle the combined wetted area of both nacelles is approximately 87 m^2, with two pylons contributing a further 10m^2. The total A320 nacelle-plus-pylon drag contribution is ΔCD0 ≈ 0.0030, representing roughly 16% of the total CD0. The eight electric motor nacelles are substantially smaller, with an estimated 0.5m diameter, and 0.8m length per streamlined pod. The total wetted area is approximately 10m^2, a reduction of nearly 90%. The interference factor is lower because the smaller pods integrate closely with the wing contour and no pylon structure is required, as the motors mount directly to the wing spar. The resulting electric nacelle drag is ΔCD0elec ≈ 0.0003. The drag contribution of the vertical tail reduces proportionally from ΔCD0VT = 0.0012 to 0.00084. Similarly, the 15% reduction in horizontal tail area reduces the horizontal tail drag component from ΔCD0HT = 0.0010 to 0.00085.

The 18% reduction in zero-lift drag, combined with the high aspect ratio enabled by extending the wingspan to the ICAO Code D limit, produces a substantial improvement in the maximum lift-to-drag ratio relative to the conventional A320. The induced drag factor is evaluated (supporting information equations 3.1-3.3), where the factor of 0.9 accounts for the sharklet-equivalent span efficiency improvement adopted at the preliminary design stage, and an Oswald efficiency of e ≈ 0.96 is assumed. This value lies at the optimistic end of the published range for commercial-class wings (e ≈ 0.80–0.96) and is justified here by three features specific to the present configuration: (i) the absence of large under-wing nacelle interference, since the eight distributed propulsors are small, streamlined and integrated tightly with the leading edge; (ii) the very high aspect ratio (AR) of 19.27, which reduces the relative contribution of tip and root losses; and (iii) the ability to optimise spanwise twist and load distribution without the structural penalty normally associated with high-AR wings, because the wing-integrated battery mass provides bending relief. For the converged 52 m design at AR = 19.27, L/D_{max} ~33, approximately 1.6× the conventional A320neo value of ∼21 and reflects the combined effect of reduced parasite drag and the much higher aspect ratio. The result is sensitive to the assumed Oswald efficiency: a more conservative value of e = 0.85 would yield an induced drag factor K ≈ 0.0175 and L/D_{max} ≈ 31, while a pessimistic e = 0.75 would give K ≈ 0.0198 and L/D_{max} ≈ 29. Even at the lower end of this range, the energy demand changes by less than 10% and the converged MTOW by less than 5%, so the design conclusions are not qualitatively sensitive to the Oswald assumption, although the headline figure should be read as an upper bound. For comparison, at the preliminary 36 m wingspan (AR ≈ 9.3), the same drag polar formulation gives L/D_{max} ≈ 23, which is comparable to a conventional A320neo and confirms that the substantial L/D gain at 52 m comes almost entirely from the aspect ratio increase rather than from the parasite drag reduction alone. Component drag estimates use representative flat-plate skin friction coefficients and Raymer form factors rather than CFD-derived values. Secondly, the tail area reductions assume that differential thrust provides adequate dynamic yaw and pitch control, which requires a detailed control system design that is beyond the scope of this study. Thirdly, propeller wake interactions with downstream surfaces are not modelled; these are expected to be second-order relative to the nacelle area reduction but warrant higher-fidelity assessment in future studies.

The electric aircraft design is derived from the A320neo airframe by removing the conventional propulsion and fuel systems and replacing them with the electric powertrain, while simultaneously applying structural material changes. The starting point is the A320 maximum zero-fuel weight (MZFW) of 60,500 kg[41] representing the maximum aircraft weight excluding usable fuel and includes the operating empty weight (OEW), payload, and all structural, systems, and furnishing mass. The A320 has a published MTOW of 73,500 kg and a wing area of 122.6 m^2[47]. The A320 is powered by two CFM56-5B turbofan engines, each with a dry mass of approximately 2,455 kg[48]. The engine pylon mass was estimated using the Roskam Class II statistical method[49], yielding 670 kg per pair. The Honeywell GTCP 131-9A Auxillary Power Unit (APU)[50] is unnecessary for electric aircraft and ground power can be supplied directly from the battery or ground power unit. Therefore, the APU and its associated fuel lines, fire suppression, and exhaust ducting are removed with an assumed mass saving of 150 kg. The A320 carries fuel in two integral wing tanks and a centre-wing box tank, with a total capacity of 15,842 litres[39]. The fuel system includes pumps, crossfeed and defuel valves, quantity indication probes, vent and pressurisation lines, and surge tanks in the wing tips. Kerosene fuel is eliminated and the wing volume is repurposed for battery modules. The integral tank structure is retained as it forms part of the primary wing structure[43] only the fuel system hardware (pumps, valves, piping) is removed. A transition to CFRP construction is assumed for the fuselage and empennage of the electric derivative, consistent with initial literature review. Component masses for the aluminium A320 baseline are taken from published structural data[51] and mass reduction percentages are applied per component. A total saving of 5,582 kg is applied to the MZFW build-up. Wing mass is treated separately and calculated following battery weight sizing within the flight model (supporting information equations 5.1-6.3). Four categories of mass are added to the electric derivative,. motors are sized from the constraint diagram power-to-weight ratio with an installation factor of 1.2 applied for nacelle, mounting structure, wiring harness, and propeller hub. For the converged design at 14.63 MW total installed power, this gives ~ 166 kg per installed motor, substantially lighter than the two turbofans they replace. Wing-integrated batteries are excluded from the structural reinforcement penalty, as the wing mass equation (supporting information equation 5.1) already accounts for inertia relief through the load relief parameter. The MZFW of the electric derivative is assembled at each iteration of the convergence loop from the A320 baseline by applying all mass removals and additions, the complete mass build up is summarised in Table 5.

Category	Item	Mass (kg)
Baseline	A320 MZFW	60,500
Removals	Turbofan engines + pylons	−5,630
	Auxiliary power unit	−150
	Fuel system hardware	−425
	CFRP fuselage/empennage saving	−5,582
	Vertical tail area reduction (30%)	−147
	Horizontal tail area reduction (15%)	−98
Additions	Electric motors (8 × installed)	+1,330
	Structural reinforcement (10% of fuselage battery and O_2 load)	Variable
	Landing gear (4.4% of MTOW)	Variable
	Thermal management (0.1 kg/kW)	Variable
Closure	MTOW = MZFW + energy system mass	—

Table 5: Mass build-up from the A320neo baseline.

B. Battery mass, placement and thermal management

Battery modules are distributed across three locations following the A-320: outboard wings, centre wing box, and fuselage cargo holds (Figure 3.2). Wing-mounted storage is preferred for three reasons; (i) spanwise battery mass provides structural bending relief, reducing root bending moments and hence wing structural mass, (ii) wing placement maintains a favourable centre-of-gravity position without the forward/aft excursions that fuselage-only storage would introduce, (iii) wing box volumes vacated by fuel tanks provide a natural integration location with existing structural containment[6]. A disadvantage of wing-integrated storage is the requirement for modular pack designs which introduces additional design and maintenance complexity. Wing structural mass was estimated using an empirical aircraft regression adapted for electric propulsion architectures[52]. The method relates wing mass fraction to aircraft loading, geometry, and structural design parameters and uses the weight of the motors and batteries calculated within the flight model for calculation of restoring moment etc. At the conceptual design level, cooling system mass is estimated at 0.1 kg/kW of installed propulsion power, consistent with published estimates for megawatt-class aerospace thermal management systems[53] . The detailed thermal design of wing-integrated cooling ducts for battery cooling is addressed in supporting information equation 6.5. Placing energy storage within the wing provides structural bending relief[15] analogous to wing-mounted fuel in conventional aircraft, this effect is captured through the battery relief load alleviation parameter, with coefficient 0.50, consistent with the Torenbeek assumption for fuel[43].

The available wing volume for battery storage is estimated using a representative supercritical airfoil. As proprietary A320 section data are unavailable, the NASA SC(2)-0714 airfoil [54] is adopted and scaled spanwise to match the published A320 thickness distribution, varying from (t/c) root = 0.152 to (t/c) tip = 0.108 [41]. The wing box is defined between 15% and 60% chord [55]. At each of 300 spanwise stations, the gross cross-sectional area is obtained via numerical integration of the airfoil ordinates. This is reduced to account for structural elements (skins, spars, caps, stringers, and ribs), four spanwise cooling ducts per bay, and a 5% allowance for systems integration and tolerances. The usable volume is then computed by trapezoidal integration along the semi-span. The resulting utilisation factor is obtained directly from the geometry, avoiding the need for empirical assumptions. Cooling duct sizing is informed by Koumakis et al.[56] which demonstrates the feasibility of forced-air cooling for wing-integrated battery systems. The wing volume is recomputed at each iteration of the convergence process, as it depends on the evolving wing geometry and MTOW. Battery packs are allocated sequentially to maximise structural efficiency. The outboard wings are filled first, as this mass provides bending relief, followed by the centre wing box at the root, which offers high volumetric capacity but no bending benefit. Any remaining battery mass is accommodated within the fuselage cargo holds using lower-efficiency, automotive-style pack configurations (Table 3). All liquid oxygen is stored in cryogenic dewar tanks within the fuselage cargo holds. The dewar volume and remaining cargo volume are computed from the parameters in Table 3 using the formulations in supporting information equations 4.11-4.15. The lower-deck cargo compartments of the A320 provide 39.5 m^3 split across forward, aft, and bulk holds[41]. In the absence of detailed finite element structural modelling, the additional structural mass required to integrate battery systems was estimated using a first-order linear scaling assumption. A structural penalty coefficient of 0.10 is applied to the installed battery mass housed in the fuselage the adopted value of 0.10 reflects a mid-range estimate for fuselage-housed battery packs positioned near the aircraft centerline [40,43].

Operation Aircraft performance is evaluated using a time-marching mission model representing a conventional short- to medium-haul flight profile, including climb, cruise, descent, and reserve segments. The trajectory and operating procedures are consistent with typical commercial operations, ensuring representativeness of A320-class missions. The model avoids classical Breguet-type assumptions by resolving all flight phases explicitly. An energy-based formulation is adopted, with performance at each timestep determined from the balance between available propulsive power and aerodynamic demand. Atmospheric variation propeller efficiency and mass depletion due to oxygen consumption are included, enabling full mission resolution without simplified range approximations (supporting information eqn 7.1-7.6). A range-matching procedure iteratively adjusts the cruise segment such that the total mission distance converges to the design range. This is embedded within an outer convergence loop updating aircraft mass, wing loading, and energy system parameters until a self-consistent solution is achieved. Battery specific energy is treated parametrically to identify technology thresholds for viable A320-class electric operation.

The mission model adopts several simplifying assumptions appropriate for conceptual design, but with associated limitations. A zero-wind condition is assumed, neglecting the impact of headwinds and tailwinds on mission time and energy consumption, and therefore underestimating operational variability. Thermal effects are not explicitly modelled; battery performance is assumed temperature-independent, with cooling represented through fixed geometric allowances rather than a coupled thermal analysis, potentially underestimating mass and power penalties. In addition, system degradation, including battery ageing and performance fade, is not considered, which would affect both mission feasibility and lifecycle performance

V.Sensitivity Analysis

Sensitivity analyses were conducted to evaluate the influence of wingspan, cruise altitude, and battery energy density on key design performance metrics. A wingspan sensitivity analysis was conducted for a 700 nm flight at Mach 0.5 with an ICA of 25,000 ft, with wingspan sweeping from 35 m to 57 m. Cruise speed and altitude were selected based on optimal performance within consequent analyses. The results of the wingspan sensitivity analysis are presented in Figure 3. Increasing wingspan from the 36 m Code C baseline to the 52 m Code D limit produces a reduction in MTOW of approximately 30–35% and a reduction in combined battery and oxygen system mass of nearly 60–65 % Figure 3c. The disproportionate reduction in battery mass relative to MTOW is a direct consequence of the nonlinear mass-energy coupling inherent to battery-electric aircraft: improving aerodynamic efficiency through a higher aspect ratio reduces induced drag, which lowers energy demand, which reduces battery mass, which in turn reduces MTOW and drag further. Wing structural mass grows from approximately 5.5 tonnes at 36 m to 10 tonnes at 52 m, Figure 3d; however, this is substantially outweighed by the battery mass savings achieved over the same range, Figure 3b. The commercial viability of the design is most directly reflected in the remaining cargo volume, which is negative below approximately 40 m, Figure 3a, indicating that battery hardware entirely displaces available payload space at short wingspans. Above 48 m, cargo volume stabilises at 25–35 m^3 and the proportion of battery housed within the wing reaches approximately 85–90 %, confirming that the 52 m configuration provides a well-packaged and commercially feasible solution. The rate of improvement diminishes beyond this point, suggesting that the Code D airport compatibility represents a practical constraint on further span extension.

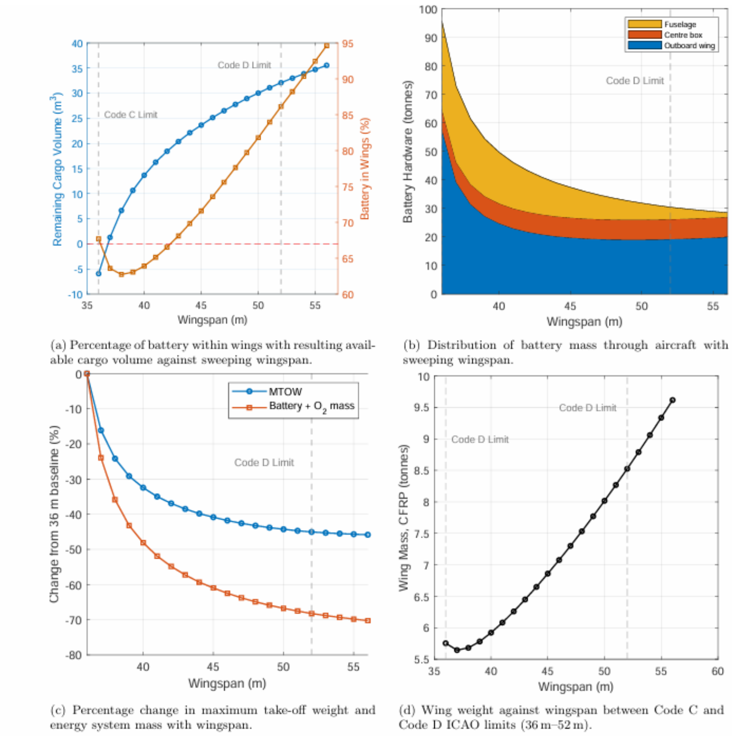

(a) Percentage of battery within wings with resulting available cargo volume against sweeping wingspan.

(b) Distribution of battery mass through aircraft with sweeping wingspan.

(c) Percentage change in maximum take-off weight and energy system mass with wingspan.

(d) Wing weight against wingspan between Code C and Code D ICAO limits (36 m–52 m).

Figure 4 – Impact of wingspan on (a) remaining cargo volume / percentage battery in the wings, (b) battery mass, (c) maximum take of weight and (d) wing mass.

The results of the cruise altitude sensitivity analysis are presented in Figure 5. Unlike a conventional turbofan aircraft, in which the thermodynamic efficiency of the Brayton cycle rewards high-altitude cruise, the performance benefit of altitude for an electric aircraft is purely aerodynamic: lower ambient density reduces drag power for a given true air speed, decreasing total energy demand and hence battery mass. This effect drives a monotonic reduction in MTOW, Figure 5b with increasing altitude for both wingspan configurations, with the steepest gradient occurring below 15,000 ft where the density ratio is high and even modest reductions in altitude incur disproportionate increases in battery mass. The principal trade-off introduced by higher cruise altitude is the requirement for a larger wing area to maintain level flight as density falls, which increases structural mass and reduces the fraction of available wing volume that can be allocated to battery storage. These effects partially oppose the mass savings from reduced energy demand, and the net outcome is captured by the remaining cargo volume, Figure 5a, which provides the most direct measure of commercial feasibility. Both configurations yield negative cargo volume below approximately 10,000–12,000 ft, confirming that low-altitude cruise is infeasible regardless of wingspan. Above 15,000 ft, the 52 m configuration provides a stable and commercially viable cargo volume of 20–40 m^3. A cruise altitude of 25,000 ft is selected as the design point, providing adequate cargo volume and a manageable wing area of approximately 140 m^2, whilst avoiding the structural and pressurisation complexity of very high-altitude operations. The energy demand at this condition and its sensitivity to battery technology assumptions are examined in the following section.

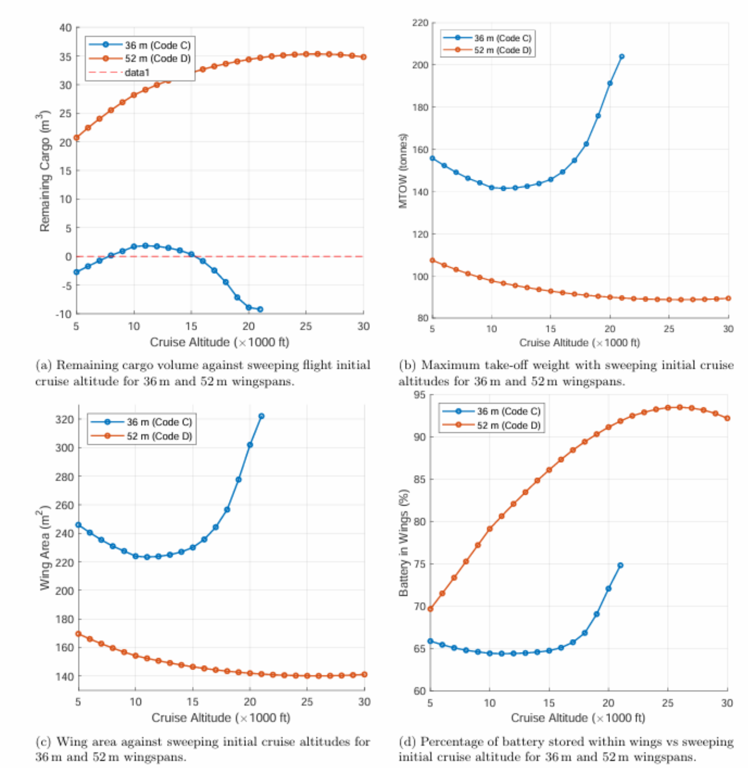

(a) Remaining cargo volume against sweeping flight initial cruise altitude for 36 m and 52 m wingspans.

(b) Maximum take-off weight with sweeping initial cruise altitudes for 36 m and 52 m wingspans.

(c) Wing area against sweeping initial cruise altitudes for 36 m and 52 m wingspans.

(d) Percentage of battery stored within wings vs sweeping initial cruise altitude for 36 m and 52 m wingspans.

Figure 5 – Interaction between wingspan and cruise altitude on (a) remaining cargo volume, (b) maximum take-off weight, (c) wing area and (d) percentage of battery in the wings.

Maximum achievable range scales approximately linearly with energy density, reaching 700 nm at 1100 Wh/kg and 850 nm at 1270 Wh/kg. Achieving 50 % of A320 range requires 2150 Wh/kg, while 75 % range (2550 nm) would require 3450 Wh/kg, both beyond current lithium–air projections. Full A320-equivalent range is therefore not achievable within any plausible near- to mid-term technology roadmap, confirming the concept is limited to short- to medium-haul operations. MTOW exhibits strong nonlinearity, Figure 6a, with peak sensitivity in the 800–1200 Wh/kg range where battery mass dominates the overall weight budget for the 700 nm design mission. The baseline value of 1150 Wh/kg lies within this high-sensitivity region, where incremental improvements in cell performance produce disproportionately large reductions in aircraft mass. The selected 52 m wingspan and 25,000 ft cruise altitude minimise mission energy demand, shifting the operating point away from this regime. In contrast, shorter span or lower cruise altitude configurations increase energy demand, moving the design back into a more sensitive region and significantly increasing dependence on battery technology. While improvements beyond 1150 Wh/kg yield substantial performance gains, returns diminish beyond 1500 Wh/kg, corresponding to approximately 40 % of the theoretical lithium–air limit.

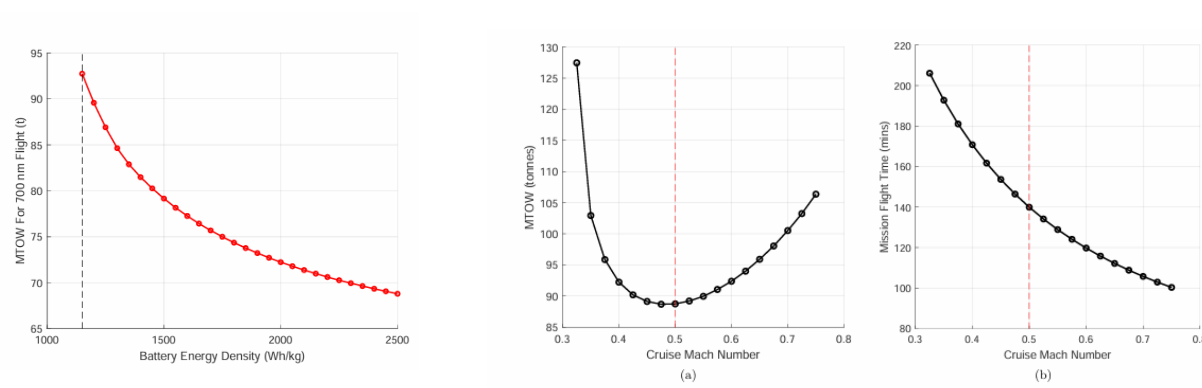

Figure 6 (a) MTOW at the 700 nm design mission as a function of battery energy density, (b) Impact of cruise Mach number on MTOW (c) Impact of cruise Mach number on 700 nm mission flight time.

An optimal cruise Mach number of 0.5 was converged throughout the design and was used for all previous sensitivity analyses. Figure 6b-c illustrate the trade-off between efficiency (MTOW) and mission time for the aircraft at 25,000ft and with a wingspan of 52m. At low Mach numbers, longer flight durations increase energy demand, while at higher Mach numbers, rising aerodynamic losses and propulsive power requirements dominate. This results in a clear optimum region in which overall aircraft mass is minimised, within which a cruise Mach of 0.5 was selected. For comparison, a conventional Airbus A320 operating at Mach 0.78 and 35,000–37,000 ft achieves a block time of approximately 110 minutes for a 700nm sector. Although only 30 minutes faster, the A320 cruises at significantly higher speed. The relatively small difference in block time is attributed to the lower cruise altitude and efficient climb performance of the propeller-driven configuration.

The sensitivity analyses show that feasibility is dominated by wingspan. Increasing span to 52m fundamentally alters the design space by reducing induced drag while providing sufficient volume for the battery and oxygen system, enabling closure on both energy and packaging constraints. In contrast, reducing the span towards the A320 baseline leads to infeasibility due to insufficient volume and increased energy demand. The selected cruise altitude of 25,000 ft and reduced cruise Mach number act as secondary optimisations, lowering power requirements and improving efficiency, but do not independently establish feasibility. At the converged design point (optimised aircraft metrics given in supporting information, Table S1), range remains limited by battery energy density, such that the concept is best interpreted as geometry-limited, with battery technology defining achievable performance within this feasible space. Achieving this configuration requires exceeding the ICAO Code C wingspan limit (36m), with the design extending into Code D. This represents a fundamental departure from the airport compatibility constraints of the A320 baseline and would reduce operational flexibility across existing narrowbody infrastructure. The feasibility of the concept is therefore contingent not only on technological advancement, but also on the adaptation of airport infrastructure.

This work has not considered the safety implications of large quantities of LOX in the cargo hold, mitigating this risk may add weight penalties for fire protection that make the design untenable. Current CS-25 regulations do not address propulsion-scale oxidiser systems[44] and LOX presents established safety risks[57]. As such we consider an alternative propulsion architecture in which oxygen is extracted from the atmosphere rather than stored onboard as LOX. This eliminates the need for cryogenic storage and associated tank volume, replacing it with an air separation unit (ASU) and compressor system supplying oxygen to the lithium-air cells. Relative to the LOX baseline, the atmospheric architecture shifts the mass-energy balance: removing 1,613 kg of stored oxygen increases battery mass from 27,376 kg to 33,030 kg due to higher electrical demand. This penalty is driven primarily by separation inefficiencies rather than compressor work[58,59]. Eliminating LOX tankage reduces dedicated volume (ASU: 0.08 m^3), but increased battery mass, Figure 7, reducing cargo capacity from 35.29 m^3 to 31.79 m^3. In addition, atmospheric supply of O_2 may not have the same purity as LOX, as such batteries with ability to operate with lower purity oxygen would be beneficial should atmospheric O_2 supply be necessary.

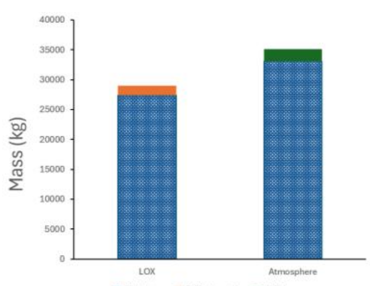

Figure 7 – Battery system mass comparison between LOX storage and atmospheric supply.

VI.Environmental and Economic Considerations

This section presents a cradle-to-gate life cycle assessment (LCA) comparing the manufacturing CO_2 emissions of the two propulsion systems: two CFM56-5B turbofans for the conventional A320, versus the Li-air battery pack, eight distributed electric motors, and cryogenic LOX supply for the electric aircraft. The airframe, landing gear, and avionics are common to both configurations and are excluded. Operation and end of life are also excluded; the objective is to quantify the manufacturing deficit that the electric aircraft must offset before yielding a net carbon benefit. Single point estimates are taken directly from published LCAs wherever possible; the only parameter for which a range is retained is the electricity grid carbon intensity, which affects LOX production and aircraft charging and is reported separately in the break-even sensitivity analysis. No published cradle-to-gate LCA exists for a production-scale Li-air battery, as the chemistry remains pre commercial. Reported factors for NMC811 pack-level emissions cluster around 74 $kgCO_{2eq}$/kWh, with a geographically resolved global range of 48 - 120 $kgCO_{2eq}$/kWh driven primarily by nickel and lithium sourcing rather than by cell assembly location[60]. Of this, approximately 40 % is attributable to cathode active-material refining and 10 % to graphite anode production[61,62]. These are the two components that are eliminated or substantially simplified in a Li-air cell. Because the Li-air cathode (porous carbon + catalyst) and metallic-lithium anode replace the two most carbon intensive components of an NMC cell, we adopt the Peisler et al. NMC811 median of 74 $kgCO_{2eq}$/kWh as the Li-air pack emission factor[60]. The uncertainty this introduces is small relative to the battery-pack sizing uncertainty and is dominated in the result by the manufacturing grid carbon intensity, which is already embedded in the published factor.

Industrial LOX is produced by cryogenic air separation; modern double-column Linde plants consume 0.42 kWh/kgLOX[58]. The resulting emission factor depends entirely on the electricity source and is therefore the one parameter retained as a function of grid intensity. For the converged 700 nm, 25000 ft, Mach 0.5 mission, LOX consumption is 1613 kg, giving approximately 144 $kgCO_{2eq}$ per flight on the EU average grid. The propulsion system comprises eight distributed permanent-magnet synchronous machines (PMSMs). The most detailed published cradle-to-gate LCA[63] of a PMSM reports 4.1 $kgCO_{2eq}$ per kilogram of finished motor for a PMSM produced on a European grid, inclusive of all materials, manufacturing energy, and assembly, this is consistent with the 110 kW industrial PMSM LCA of Auer & Meincke[64]. Applied to a 13.2 kW/kg aerospace-grade machine, the installed factor is: emotor,installed = 0.37 $kgCO_{2eq}$/kW. Adding the SiC inverter and thermal-management contribution of 2.6 $kgCO_{2eq}$/kW for the power-electronics subsystem[63] gives a rounded installed factor of 3kgCO2eq/kW, which is used directly. Manufacturing accounts for 0.089% of total lifecycle impact of an A320[65], with the wing and engines dominating this phase[66]. Disaggregated results indicate that the two CFM56-5B engines contribute approximately 40,000 $kgCO_{2eq}$ per engine, this value, derived directly from a factory-level LCA[65], is adopted here. The battery pack contributes approximately 97 % of the electric aircraft's manufacturing footprint, overwhelmingly dominated by the 20848 kWh of installed cell capacity at 74 $kgCO_{2eq}$/kWh. The break-even number of flights is given by equation 2.

$$N_{\text{break-even}} = \frac{\Delta CO_{2,\text{mfg}}}{CO_{2,\text{kerosene}} - CO_{2,\text{LOX}} - CO_{2,\text{grid}}} \qquad \text{Eqn 2}$$

For a 700nm mission, the A320ceo (CFM56-5B) produces approximately 17380 $kgCO_2$ per flight based on a fuel burn of 5500 kg and an emission index of 3.16 $kgCO_2$/kg (Airbus, 2021a). The more efficient A320neo reduces fuel burn by approximately 15 %, giving 14773 $kgCO_2$ per flight (Airbus, 2021a). For the electric aircraft, per-flight emissions arise from grid electricity used for battery charging (14,338 kWh including charging losses) and liquid oxygen production (677 kWh equivalent), making break-even highly dependent on grid carbon intensity, Figure 8a.

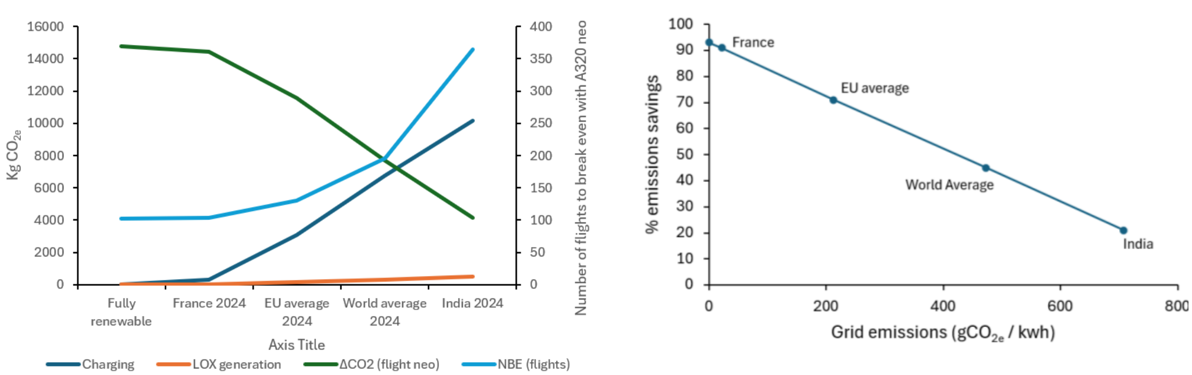

Figure 8 (a) Impact of grid emissions on number of flights to break even with A320neo. (b) Impact of grid emissions on % emissions savings compared with the A320neo.

In the limiting case of a fully coal-based grid (~1,000 g CO_2/kWh), per-flight emissions exceed those of the A320neo, and lifecycle break-even is no longer achievable. However, no real-world national grid currently exceeds the threshold at which break-even becomes infeasible. Overall, the electric aircraft achieves lifecycle emissions break-even across all realistic grid scenarios, although the margin is strongly dependent on electricity decarbonisation, Figure 8a. The flight-count break-even metric does not capture full lifecycle effects, namely cumulative kerosene combustion and repeated battery manufacture, with a 1,500-cycle life and utilisation of 2,040 flights per year, the battery pack is replaced 27 times over 20 years, giving 28 packs in total, while conventional aircraft retain their original engines. During a 20-year lifecycle, the electric aircraft achieves substantial emissions reductions, reaching approximately 94% relative to the A320ceo and 93% relative to the A320neo on near-renewable grids, Figure 8b. However, savings decrease markedly with grid carbon intensity, falling to 45% (world average) and 21% (India) against the A320neo. While the electric aircraft remains beneficial in all realistic cases, the reduced margin highlights battery cycle life as the dominant factor in lifecycle performance.

There are several limitations on this analysis, in particular that the environmental impacts of the batteries are not modelled on Li-air specific data and do not include any reduction in manufacturing emissions over the 20-year lifespan of the aircraft. The 1500-cycle battery life used in the 20-year comparison is itself uncertain: laboratory Li-air cells have demonstrated anywhere from 500 to over 2000 cycles depending on cathode catalyst and electrolyte chemistry. End of-life recycling credits (60–65% for Li-ion cells, up to 95% for Ni superalloys[67,68] are excluded throughout; because battery manufacturing dominates the electric lifetime footprint, even modest recycling credits on the 28 pack replacements would substantially improve the environmental case. Non-CO_2 climate effects of kerosene combustion such as contrails, NOx-induced ozone, and soot are also excluded and would further strengthen the electric case, particularly on cleaner grids.

C. Operating Cost Comparison.

The direct operating cost (DOC) per flight and the cumulative 20-year total cost of ownership for the design aircraft is compared with the conventional A320ceo. The cost model captures the six principal DOC components: energy (fuel or electricity and LOX), propulsion system maintenance, airframe maintenance, battery replacement, flight crew, and airport charges. Costs common to both configurations (passenger service, marketing, administration) are excluded. Figure 9a provides a comparison of the DOC of the electric version with the A320 ceo (neo data unavailable). A utilisation of 2,040 flights per year is assumed, corresponding to six flights per day over 340 operating days, representative of a short-haul single aisle aircraft in European or US domestic service. Each flight is a 700 nm mission at the design point established by the integrated sizing model. A320ceo fuel consumption is approximately 5,500 kg of Jet-A1, for a 150-seat configuration at 85 % load factor [69]. At a Jet-A1 price of $0.85/kg ($2.70 per US gallon) fuel cost is $ 4,675 per flight [70]. With a 92% grid to-battery charging efficiency, grid energy draw per flight for the electric aircraft is 14338 kWh, with an industrial electricity cost of $0.10 /kWh [71], leads to $1434 electricity per flight. LOX consumption is 1613 kg per flight at $0.15 /kg delivered[72], giving a LOX cost of $242 per flight, Figure 9a. The CFM56 maintenance programme comprises scheduled shop visits, life-limited part (LLP) replacements, and on-wing line maintenance. CFM56 engines typically achieve 15,000–20,000 flight hours before their first shop visit, driven by exhaust gas temperature (EGT) margin erosion[73]. A full performance restoration shop visit costs approximately $3.0–5.0M per engine, depending on work scope and the extent of LLP replacement; LLP sets alone cost approximately $1.5–2.0M per engine per cycle[74,75]. On-wing line maintenance (borescope inspections, oil system servicing, accessory replacements) adds a further $80–120 per flight hour. The industry-standard metric for engine maintenance, repair and overhaul (MRO) budgeting is the reserve rate per engine flight hour (EFH). For two CFM56 engines on a short-haul cycle (1.5 EFH per flight cycle), the combined rate is approximately $ 600–900 /EFH, with a representative central value of $ 750 /EFH. At 3.5 block hours per flight, engine MRO costs $2,625 per flight. Electric motors are fundamentally simpler than gas turbines: no combustion system, no hot-section components subject to creep and oxidation, no oil system, and no compressor susceptible to foreign object damage. The principal wear items are bearings (replacement interval ~30,000 hours) and winding insulation. For electrified aircraft propulsion maintenance costs of $10 per motor per flight hour were assumed, for eight motors at 3.5 block hours, motor maintenance is $280 per flight. The cryogenic LOX distribution system adds a further $105 per flight at $30 /FH, giving a combined propulsion maintenance cost of $385 per flight. The A320 airframe maintenance programme is structured around A-checks at approximately 750 FH and base/C check intervals of approximately 7,500 FH[76].

When combined with major component overhaul costs, the total airframe maintenance burden is approximately $400–600 /FH [77]; a central value of $500 /FH is adopted, giving $1,750 per flight for the conventional. The electric aircraft's airframe requires the same phased inspection programme. Several systems are absent (APU, fuel tanks, fuel plumbing), reducing each check scope, but the battery thermal management system and high-voltage distribution system introduce new requirements. Analogous assumptions for battery-electric aircraft by Hepperle[21] and in the NASA N+3 technology roadmap[78] suggest net airframe maintenance reductions of 10–20% for propulsion-related inspections. A net rate of $400 /FH is adopted. Regarding battery degradation, an assumption of 1,500 cycles is adopted at 2,040 flights per year, a 1,500-cycle battery requires replacement approximately 1.36 times per year. The pack-level cost is estimated at $150 /kWh, consistent with projected 2030s battery costs[79]. For the 20848 kWh pack this yields $2,085 per flight. At 800 cycles the cost rises to $3,909 per flight; at 2,500 cycles it falls to $1,251. An all-in crew cost of $400/FH is assumed. and a representative European landing fee of $8/tonne MTOW[77]. Navigation charges $800/flight and ground handling $1500/flight are equal for both, giving total airport charges of $2924 (conventional) and $3010 (electric) per flight, Figure 9a. The electric aircraft achieves a 25% reduction in DOC per flight. The saving is driven primarily by the elimination of kerosene and the substantial reduction in propulsion maintenance, which outweigh the additional battery replacement cost and slightly higher airport charges. Flight crew cost is lower for the conventional aircraft due to its shorter block time. Over a 20-year service life at 2,040 flights per year (six sectors per day over 340 operating days [77], the total direct operating and fixed costs are summarised in Figure 9b. Fixed costs comprise straight-line depreciation ($5.5M/yr conventional, $7.0 M/yr electric, based on acquisition costs of $110M and $140M respectively and hull insurance at $0.8M /$1.0M per year, consistent with a 1–2% of hull value premium [69].

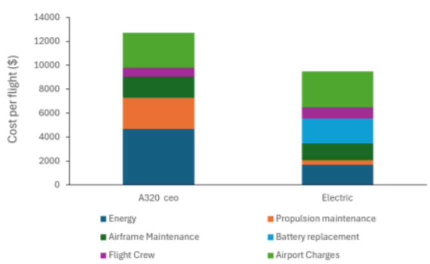

Cost Category	Conv. A320ceo (USD M)	Electric A320 (USD M)
Energy (20 yr)	190.7	68.4
Propulsion maintenance (20 yr)	107.1	15.7
Airframe maintenance (20 yr)	71.4	57.1
Battery replacement (20 yr)	—	85.1
Flight crew (20 yr)	30.0	38.0
Airport charges (20 yr)	119.3	122.8
Insurance (20 yr, $0.8 M/$1.0 M p.a.)	16.0	20.0
Depreciation (20 yr)	110.0	140.0
20-year total	**644.5**	**547.1**
Saving		**$97.4 M (15.1%)**

Table 5.6: 20-year total cost of ownership — 700 nm mission.

Figure 9 (a) DOC per flight for the A320 neo compared with an electric version. (b) 20 year cost of ownership of A320 with electric version.

The electric aircraft saves $97.4M over 20 years, a 15% reduction in total cost of ownership. The saving is dominated by energy ($122M) and propulsion maintenance ($91M), driven by the elimination of kerosene and turbofan MRO[76] respectively. These gains are partially offset by battery replacement ($85.1M at 1,500 cycles [10,9]) higher depreciation ($30M), and increased crew costs from the longer Mach 0.5 block time [77]. The saving is slightly reduced relative to the per-flight comparison because these fixed and time-based costs compound across the full-service life. The cost comparison is most sensitive to jet fuel price, battery cycle life, and electricity price. The electric aircraft is cheaper per flight at every historically observed jet fuel price with a break-even price of $0.23/kg, well below the modern-era minimum of $0.30/kg[80]. Battery cycle life has the largest single effect: at 800 cycles the per-flight battery cost rises to $3,909, reducing the saving to 12%; at 2,500 cycles it falls to $1,251, increasing the saving to 32%. The $30M acquisition cost premium has limited impact, adding only $1.5M/yr when amortised.

VII.Recommendations and Further Work

The present study establishes a self-consistent 700 nm electric narrow-body concept at the conceptual level; however, several areas require higher-fidelity analysis before progression to preliminary design. The following recommendations are grouped by modelling fidelity and ordered by the magnitude of uncertainty they address.

The most significant unresolved issue is the safety case for carrying approximately 1613 kg of LOX, roughly 300 times the oxidiser mass of a conventional A320 crew oxygen system[41]. Unlike conventional systems, no certification exists for propulsion scale cryogenic oxidiser storage in a pressurised. LOX introduces severe ignition hazards, while its interaction with lithium-metal battery thermal runaway presents a novel combined hazard. Existing CS-25 requirements address only breathing oxygen systems and do not cover propulsion-scale oxidiser storage [81]. Further work should establish a safety framework covering LOX containment integrity, ground handling, in flight failure modes, and the certification pathway under CS-25 or equivalent Special Conditions. If such analysis precludes large-scale onboard LOX, the atmospheric oxygen extraction architecture would need reconsideration, accepting its associated compressor power penalty, mass, drag, and sizing impacts. A comparative systems-level trade study between closed-LOX and open-air architectures is therefore a priority.

Lithium-metal batteries remain a critical safety uncertainty due to their higher reactivity, unproven pack-scale abuse tolerance, and the risk of cascading thermal runaway within a 20848 kWh pack integrated into a composite wing. Further work should address: (i) pack-level thermal abuse testing to quantify heat release and propagation; (ii) fire suppression and containment, including interaction with nearby LOX storage; and (iii) development of transport-category battery safety standards. Outcomes would feed back into structural reinforcement, containment mass, and battery placement.

Drag polar is based on representative skin-friction coefficients and Raymer form factors. This should be validated using an actuator-disc CFD study of the converged planform. Such analysis would quantify propeller–wing interaction effects at the eight leading-edge propulsors, including high-lift augmentation and nacelle–wing interference drag, as well as propeller compressibility losses at $M \approx 0.5$. Stability, control and propulsion architecture. The assumed 30% vertical tail and 15% horizontal tail reductions rely on differential thrust for yaw control and remain unvalidated. Recommended work includes: (i) development of a six-degree-of-freedom flight dynamics model with spanwise-resolved thrust; (ii) demonstration of controllability under critical failure cases (motor loss, asymmetric power, inverter failure) within CS-25 handling qualities; and (iii) reassessment of empennage sizing if required.

The key assumption of a 1,150 Wh/kg solid-state Li–air cell with 1,500 cycle life is based on laboratory-scale data and remains unproven at pack level. Commercial viability is sensitive to cycle life below 1,000 cycles. Experimental work is required to validate (i) specific energy at aviation-relevant C-rates, (ii) cycle and calendar life across flight temperatures, and (iii) pack-level integration with the LOX system. A dedicated Li–air life-cycle assessment is also needed, as the current analysis uses NMC811 as a proxy.

The flight model assumes zero wind, isothermal battery behaviour, and no calendar degradation. Future work should include: (i) representative wind and temperature profiles; (ii) a coupled electro-thermal battery model to replace the current 0.1 kg/kW cooling estimate; and (iii) fleet-level utilisation modelling incorporating charging, LOX refueling, and reduced cruise Mach. The latter is critical, as the additional 30 minutes per 700 nm sector relative to the A320 affects achievable utilisation beyond the current cost model. Configuration-level alternatives. The tube-and-wing configuration was selected for reduced development risk. A blended wing body offers a higher-efficiency alternative, with reported 20–30% improvements in L/D [82,83], increased internal volume, and improved battery integration. Combined with boundary-layer ingestion [20,84], this could extend range beyond 700 nm at the same technology level. However, certification, manufacturing, and passenger acceptance challenges place BWB configurations in a longer-term development horizon.

VIII.Conclusions

A short-haul, 150-seat, lithium–air-powered narrow-body aircraft derived from the A320 is technically feasible at a 700 nm design range, contingent on four enabling technologies: 1150 Wh/kg lithium–air cells with ≥ 1500 cycle life, 13 kW/kg electric motors, certified distributed electric propulsion, and a viable safety and certification pathway for large-scale onboard liquid oxygen storage. These are consistent with a 2030–2035 horizon but remain unproven at production scale. The converged design has an MTOW 14 % above the A320ceo, requires a 52 m (ICAO Code D) wing, and operates at Mach 0.5 and 25000 ft to maximise efficiency. It retains 89 % of cargo volume and covers 76% of Heathrow A320 departures by frequency. Commercially, the aircraft achieves a 26 % per-flight cost reduction relative to the A320ceo (approximately $105 M over 20 years) and reduces lifecycle CO_2 emissions by 45 % relative to the A320neo on the world average grid, rising to over 90 % on low-carbon grids. The principal barriers are external to the aircraft, namely high-power airport charging, LOX supply, and a novel certification pathway. The concept is therefore best viewed as a late-2030s target rather than a near-term solution, but presents a compelling technical, economic, and environmental case for continued development.

Funding Sources

Institute of Sustainability and Climate Change, University of Bath.
Department of Mechanical Engineering, Faculty of Engineering and Design, University of Bath

References

[1] Lee, D. S., Fahey, D. W., Skowron, A., Allen, M. R., Burkhardt, U., Chen, Q., Doherty, S. J., Freeman, S., Forster, P. M., Fuglestvedt, J., Gettelman, A., De León, R. R., Lim, L. L., Lund, M. T., Millar, R. J., Owen, B., Penner, J. E., Pitari, G., Prather, M. J., Sausen, R., and Wilcox, L. J., "The Contribution of Global Aviation to Anthropogenic Climate Forcing for 2000 to 2018," *Atmospheric Environment*, Vol. 244, 2021, p. 117834. https://doi.org/10.1016/j.atmosenv.2020.117834

[2] Bergero, C., Gosnell, G., Gielen, D., Kang, S., Bazilian, M., and Davis, S. J., "Pathways to Net-Zero Emissions from Aviation," *Nature Sustainability*, Vol. 6, No. 4, 2023, pp. 404–414. https://doi.org/10.1038/s41893-022-01046-9

[3] Nykvist, B., and Nilsson, M., "Rapidly Falling Costs of Battery Packs for Electric Vehicles," *Nature Climate Change*, Vol. 5, No. 4, 2015, pp. 329–332. https://doi.org/10.1038/nclimate2564

[4] Wild, M., O'Neill, L., Zhang, T., Purkayastha, R., Minton, G., Marinescu, M., and Offer, G. J., "Lithium Sulfur Batteries, a Mechanistic Review," *Energy & Environmental Science*, Vol. 8, No. 12, 2015, pp. 3477–3494. https://doi.org/10.1039/C5EE01388G

[5] Deng, J., Bae, C., Denlinger, A., and Miller, T., "Electric Vehicles Batteries: Requirements and Challenges," *Joule*, Vol. 4, No. 3, 2020, pp. 511–515. https://doi.org/10.1016/j.joule.2020.01.013

[6] Hasan, M. M., Haque, R., Jahirul, M. I., Rasul, M. G., Fattah, I. M. R., Hassan, N. M. S., and Mofijur, M., "Advancing Energy Storage: The Future Trajectory of Lithium-Ion Battery Technologies," *Journal of Energy Storage*, Vol. 120, 2025, p. 116511. https://doi.org/10.1016/j.est.2025.116511

[7] Tiede, B., O'Meara, C., and Jansen, R., "Battery Key Performance Projections Based on Historical Trends and Chemistries," presented at the 2022 IEEE/AIAA Transportation Electrification Conference and Electric Aircraft Technologies Symposium (ITEC+EATS), 2022. https://doi.org/10.1109/ITEC53557.2022.9814008

[8] Bruce, P. G., Freunberger, S. A., Hardwick, L. J., and Tarascon, J.-M., "Li–O2 and Li–S Batteries with High Energy Storage," *Nature Materials*, Vol. 11, No. 1, 2012, pp. 19–29. https://doi.org/10.1038/nmat3191

[9] Imanishi, N., and Yamamoto, O., "Rechargeable Lithium–Air Batteries: Characteristics and Prospects," *Materials Today*, Vol. 17, No. 1, 2014, pp. 24–30. https://doi.org/10.1016/j.mattod.2013.12.004

[10] Luntz, A. C., and McCloskey, B. D., "Nonaqueous Li–Air Batteries: A Status Report," *Chemical Reviews*, Vol. 114, No. 23, 2014, pp. 11721–11750. https://doi.org/10.1021/cr500054y

[11] Kwak, W.-J., Rosy, Sharon, D., Xia, C., Kim, H., Johnson, L. R., Bruce, P. G., Nazar, L. F., Sun, Y.-K., Frimer, A. A., Noked, M., Freunberger, S. A., and Aurbach, D., "Lithium–Oxygen Batteries and Related Systems: Potential, Status, and Future," *Chemical Reviews*, Vol. 120, No. 14, 2020, pp. 6626–6683. https://doi.org/10.1021/acs.chemrev.9b00609

[12] Zhu, Q., Ma, J., Li, S., and Mao, D., "Solid-State Electrolyte for Lithium-Air Batteries: A Review," *Polymers*, Vol. 15, No. 11, 2023, p. 2469. https://doi.org/10.3390/polym15112469

[13] Kondori, A., Esmaeilirad, M., Harzandi, A. M., Amine, R., Saray, M. T., Yu, L., Liu, T., Wen, J., Shan, N., Wang, H.-H., Ngo, A. T., Redfern, P. C., Johnson, C. S., Amine, K., Shahbazian-Yassar, R., Curtiss, L. A., and Asadi, M., "A Room Temperature Rechargeable Li2O-Based Lithium-Air Battery Enabled by a Solid Electrolyte," *Science*, Vol. 379, No. 6631, 2023, pp. 499–505. https://doi.org/10.1126/science.abq1347

[14] Lin, T., "A Novel Class of High-Energy/Power-Density, Long-Cycle-Life, Roll to-Roll-Processed Solid-State Lithium-Air Batteries (SSLaB) for Aviation Applications," presented at the PROPEL-1K Program Annual Meeting, 2025.

[15] Wang, Z., De Breuker, R., Sodja, J., Wolleswinkel, R. E., de Vries, R., and Giuffré, A., "A Study on Wing Structural Design and Sizing for a Large Battery-Electric Aircraft," *AIAA AVIATION FORUM AND ASCEND 2025*, American Institute of Aeronautics and Astronautics, 2025. https://doi.org/10.2514/6.2025-3470

[16] Karadotcheva, E., Nguyen, S. N., Greenhalgh, E. S., Shaffer, M. S. P., Kucernak, A. R. J., and Linde, P., "Structural Power Performance Targets for Future Electric Aircraft," *Energies*, Vol. 14, No. 19, 2021, p. 6006. https://doi.org/10.3390/en14196006
[17] "'Spirit of Innovation' Stakes Claim to Be the World's Fastest All-Electric Vehicle." Retrieved 11 August 2026. https://www.rolls-royce.com/media/press-releases/2021/19-11-2021-spirit-of-innovation-stakes-claim-to-be-the-worlds-fastest-all-electric-vehicle.aspx
[18] "H3X Technologies | HPDM-350." Retrieved 11 August 2026. https://www.h3x.tech/products/hpdm-350
[19] "Electric Machines." Retrieved 11 August 2026. https://www.nasa.gov/eap-technology/electric-machines/
[20] Hall, C., Pastra, C. L., Burrell, A., Gladin, J., and Mavris, D. N., "Projecting Power Converter Specific Power Through 2050 for Aerospace Applications," presented at the 2022 IEEE/AIAA Transportation Electrification Conference and Electric Aircraft Technologies Symposium (ITEC+EATS), 2022. https://doi.org/10.1109/ITEC53557.2022.9813991
[21] Hepperle, M., "Electric Flight – Potential and Limitations," 2012. https://doi.org/10.14339/STO-MP-AVT-209-09-pdf
[22] "Subsonic Ultra Green Aircraft Research: Phase 2: Hybrid Electric Design Exploration - Volume 2 - NASA Technical Reports Server (NTRS)." Retrieved 11 August 2026. https://ntrs.nasa.gov/citations/20150017039
[23] Wenping Cao, Mecrow, B. C., Atkinson, G. J., Bennett, J. W., and Atkinson, D. J., "Overview of Electric Motor Technologies Used for More Electric Aircraft (MEA)," *IEEE Transactions on Industrial Electronics*, Vol. 59, No. 9, 2012, pp. 3523–3531. https://doi.org/10.1109/TIE.2011.2165453
[24] Raymer, D. P., "Aircraft Design: A Conceptual Approach," American Institute of Aeronautics and Astronautics, Inc, Reston, VA, 2018.
[25] McCormick, B. W., "Aerodynamics, Aeronautics, and Flight Mechanics," Wiley, New York, 1995.
[26] "The Jet Engine, 5th Edition | Wiley," Wiley.com. Retrieved 11 August 2026. https://www.wiley.com/en-gb/the-jet-engine-5th-edition-p-9781119065999
[27] Kim, H. D., Perry, A. T., and Ansell, P. J., "A Review of Distributed Electric Propulsion Concepts for Air Vehicle Technology," presented at the 2018 AIAA/IEEE Electric Aircraft Technologies Symposium (EATS), 2018.
[28] Keller, D., "Numerical Study on Lift Augmentation via Distributed Propulsion for a Propeller-Driven Regional Transport Aircraft in Landing Configuration," *CEAS Aeronautical Journal*, Vol. 17, No. 2, 2026, pp. 553–566. https://doi.org/10.1007/s13272-025-00863-w
[29] Patterson, M. D., Borer, N. K., and German, B., "A Simple Method for High-Lift Propeller Conceptual Design," presented at the 54th AIAA Aerospace Sciences Meeting, 2016. https://doi.org/10.2514/6.2016-0770
[30] Borer, N. K., Patterson, M. D., Viken, J. K., Moore, M. D., Clarke, S., Redifer, M. E., Christie, R. J., Stoll, A. M., Dubois, A., Bevirt, J., Gibson, A. R., Foster, T. J., and Osterkamp, P. G., "Design and Performance of the NASA SCEPTOR Distributed Electric Propulsion Flight Demonstrator," presented at the American Inst. of Aeronautics and Astronautics, 2016.
[31] Stoll, A. M., Bevirt, J., Moore, M. D., Fredericks, W. J., and Borer, N. K., "Drag Reduction Through Distributed Electric Propulsion," presented at the 14th AIAA Aviation Technology, Integration, and Operations Conference, 2014. https://doi.org/10.2514/6.2014-2851
[32] Viswanathan, V., Epstein, A. H., Chiang, Y.-M., Takeuchi, E., Bradley, M., Langford, J., and Winter, M., "The Challenges and Opportunities of Battery-Powered Flight," *Nature (London)*, Vol. 601, No. 7894, 2022. https://doi.org/10.1038/s41586-021-04139-1
[33] Vries, R. de, Wolleswinkel, R. E., Hoogreef, M., and Vos, R., "A New Perspective on Battery-Electric Aviation, Part II: Conceptual Design of a 90-Seater," *AIAA SCITECH 2024 Forum*, American Institute of Aeronautics and Astronautics. https://doi.org/10.2514/6.2024-1490
[34] Silva, C. I. da, Alonso, J. J., Orra, T. H., and Vegh, J. M., "Flight Path and Wing Optimization of Lithium-Air Battery Powered Passenger Aircraft," *53rd AIAA Aerospace Sciences Meeting*, 2015. https://doi.org/10.2514/6.2015-1674
[35] Vegh, J. M., Alonso, J. J., Orra, T. H., and Ilario Da Silva, C., "Flight Path and Wing Optimization of Lithium-Air Battery Powered Passenger Aircraft," presented at the 53rd AIAA Aerospace Sciences Meeting, 2015. https://doi.org/10.2514/6.2015-1674
[36] Ali, U., Okasha, M., Dief, T. N., ElSayed, M. S. A., and Kamra, M. M., "Blended Wing Body Designs for Aerodynamic, Stability, and Control Optimization: A Comprehensive Review," *Transportation Engineering*, Vol. 22, 2025, p. 100397. https://doi.org/10.1016/j.treng.2025.100397
[37] Baker, A. A., Dutton, S., and Kelly, D. W., "Composite Materials for Aircraft Structures, Second Edition," American Institute of Aeronautics and Astronautics, 2004.

[38] "OpenSky." Retrieved 31 August 2026. https://opensky-network.org/
[39] "ATA 35: Airbus A320 (Technical Notes) - AviationHunt," Sept 24 2023. Retrieved 31 August 2026. https://www.aviationhunt.com/airbus-a320-ata-35/
[40] Raymer, D., "Aircraft Design: A Conceptual Approach, Sixth Edition," American Institute of Aeronautics and Astronautics, Inc., Washington, DC, 2018. https://doi.org/10.2514/4.104909
[41] Airbus S.A.S., "A320 Family: Aircraft Characteristics — Airport and Maintenance Planning'. Revision 41," 2024.
[42] "A400M | Military Aircraft | Defence | Airbus," June 12 2024. Retrieved 31 August 2026. https://www.airbus.com/en/products-services/defence/military-aircraft/a400m
[43] Torenbeek, E., "Advanced Aircraft Design: Conceptual Design, Analysis and Optimization of Subsonic Civil Airplanes," Wiley, 2013. https://doi.org/10.1002/9781118568101
[44] "Official Publication: Certification Specifications (CSs) / Detailed Specifications (DSs) | EASA." Retrieved 31 August 2026. https://www.easa.europa.eu/en/official-publication/certification-specifications
[45] "Electric Machines." Retrieved 31 August 2026. https://www.nasa.gov/eap-technology/electric-machines/
[46] Cao, W., Mecrow, B. C., Atkinson, G. J., Bennett, J. W., and Atkinson, D. J., "Overview of Electric Motor Technologies Used for More Electric Aircraft (MEA)," *IEEE Transactions on Industrial Electronics*, Vol. 59, No. 9, 2012, pp. 3523–3531. https://doi.org/10.1109/TIE.2011.2165453
[47] "Airport Operations and Aircraft Characteristics | Airbus," Oct 24 2024. Retrieved 31 August 2026. https://www.aircraft.airbus.com/en/customer-care/fleet-wide-care/airport-operations-and-aircraft-characteristics
[48] European Union Aviation Safety Agency, "Type-Certificate Cfm56-5b and Cfm56-5c Series Engines," Jan2023.
[49] Roskam, D. J., "Airplane Design Part V: Component Weight Estimation: Volume 5," Design, Analysis and Research Corporation, Lawrence, Kansas, 2003.
[50] "131 Series Auxiliary Power Units | Honeywell." Retrieved 31 August 2026. https://www.honeywellaerospace.com/us/en/products-and-services/products/power-and-propulsion/auxiliary-power-units/131-series-auxiliary-power-units
[51] "Airbus A320-100 Performance | Aircraft Investigation Info | Passenger Aircraft." Retrieved 31 August 2026. https://aircraftinvestigation.info/airplanes/A320-100.html#google_vignette
[52] "Evaluation of the Mass and Aerodynamic Efficiency of a High Aspect Ratio Wing for Prospective Passenger Aircraft." Retrieved 31 August 2026. https://www.mdpi.com/2226-4310/9/9/497
[53] Chin, J. C., Look, K., McNichols, E. O., Hall, D. L., Gray, J. S., and Schnulo, S. L., "Battery Cell-to-Pack Scaling Trends for Electric Aircraft," presented at the AIAA/IEEE Electric Aircraft Technologies Symposium (EATS).
[54] Harris, D., "NASA Supercritical Airfoils."
[55] Niu, C., and Niu, M. C.-Y., "Airframe Structural Design: Practical Design Information and Data on Aircraft Structures," Conmilit Press, 1988.
[56] Koumakis, D., Joiner, K. F., Hill, D., Zhao, J., and Khraibut, A., "CFD-Based Viability for Safely Cooling Wing-Mounted High-Performance Batteries in an after-Market Aircraft Electrification," *Aircraft Engineering and Aerospace Technology*, Vol. 97, No. 11, 2025, pp. 9–19. https://doi.org/10.1108/AEAT-03-2025-0096
[57] Wicki, R., "Liquid Oxygen – Fire Hazards of Oxygen and Oxygen-Enriched Atmospheres," *CHIMIA*, Vol. 57, No. 12, 2003, pp. 781–781. https://doi.org/10.2533/000942903777678425
[58] Smith, A. R., and Klosek, J., "A Review of Air Separation Technologies and Their Integration with Energy Conversion Processes," *Fuel Processing Technology*, Vol. 70, No. 2, 2001, pp. 115–134. https://doi.org/10.1016/S0378-3820(01)00131-X
[59] "Yvc Rao.Pdf," Google Docs. Retrieved 31 August 2026. https://docs.google.com/file/d/0BzCmwoVStdgOZkpLSDV2QThqd2M/edit?usp=embed_facebook
[60] Peiseler, L., Schenker, V., Schatzmann, K., Pfister, S., Wood, V., and Schmidt, T., "Carbon Footprint Distributions of Lithium-Ion Batteries and Their Materials," *Nature Communications*, Vol. 15, No. 1, 2024, p. 10301. https://doi.org/10.1038/s41467-024-54634-y
[61] "Life Cycle Analysis of Lithium-Ion Batteries for Automotive Applications." Retrieved 1 September 2026. https://www.mdpi.com/2313-0105/5/2/48
[62] Llamas-Orozco, J. A., Meng, F., Walker, G. S., Abdul-Manan, A. F. N., MacLean, H. L., Posen, I. D., and McKechnie, J., "Estimating the Environmental Impacts of Global Lithium-Ion Battery Supply Chain: A Temporal, Geographical, and Technological Perspective," *PNAS Nexus*, Vol. 2, No. 11, 2023, p. pgad361. https://doi.org/10.1093/pnasnexus/pgad361

[63] Nordelöf, A., Grunditz, E., Lundmark, S., Tillman, A.-M., Alatalo, M., and Thiringer, T., "Life Cycle Assessment of Permanent Magnet Electric Traction Motors," *Transportation Research Part D: Transport and Environment*, Vol. 67, 2019, pp. 263–274. https://doi.org/10.1016/j.trd.2018.11.004
[64] Auer, J., and Meincke, A., "Comparative Life Cycle Assessment of Electric Motors with Different Efficiency Classes: A Deep Dive into the Trade-Offs between the Life Cycle Stages in Ecodesign Context," *The International Journal of Life Cycle Assessment*, Vol. 23, No. 8, 2018, pp. 1590–1608. https://doi.org/10.1007/s11367-017-1378-8
[65] Howe, S., Kolios, A. J., and Brennan, F. P., "Environmental Life Cycle Assessment of Commercial Passenger Jet Airliners," *Transportation Research Part D: Transport and Environment*, Vol. 19, 2013, pp. 34–41. https://doi.org/10.1016/j.trd.2012.12.004
[66] Jemioło, W., "University of Nordland, Bodø, Norway."
[67] Harper, G., Sommerville, R., Kendrick, E., Driscoll, L., Slater, P., Stolkin, R., Walton, A., Christensen, P., Heidrich, O., Lambert, S., Abbott, A., Ryder, K., Gaines, L., and Anderson, P., "Recycling Lithium-Ion Batteries from Electric Vehicles," *Nature*, Vol. 575, No. 7781, 2019, pp. 75–86. https://doi.org/10.1038/s41586-019-1682-5
[68] Environment, U. N., "Recycling Rates of Metals: A Status Report | UNEP - UN Environment Programme," Apr 28 2011. Retrieved 1 September 2026. https://www.unep.org/resources/report/recycling-rates-metals-status-report
[69] "ICAO Aircraft Engine Emissions Databank | EASA." Retrieved 1 September 2026. https://www.easa.europa.eu/en/domains/environment/icao-aircraft-engine-emissions-databank
[70] "Jet Fuel Price Monitor." Retrieved 1 September 2026. https://www.iata.org/en/publications/economics/fuel-monitor/
[71] "[Nrg_pc_205_c] Electricity Prices Components for Non-Household Consumers - Annual Data (from 2007 Onwards)." Retrieved 1 September 2026. https://ec.europa.eu/eurostat/databrowser/view/NRG_PC_205_C/default/table?lang=en
[72] "Oxygen Prices 2026 | August Price Chart, Trend & Forecast." Retrieved 1 September 2026. https://www.imarcgroup.com/oxygen-pricing-report
[73] "CFM56-7B Maintenance Costs & Reserves Analysis," *Aircraft Commerce*, No. 39, 2005, pp. 35–42.
[74] "CFM56-5A/-5B Maintenance Analysis & Budget, Issue 50 Feb/Mar 2007," Aircraft Commerce. Retrieved 7 September 2026. https://aircraftcommerceevents.com/article/aircraft-owners-operators-guide/cfm56-5a-5b-maintenance-analysis-budget-issue-50-feb-mar-2007/
[75] "Magnetic Expects CFM56 Market Challenges, Opportunities In 2024 | Aviation Week." Retrieved 7 September 2026. https://aviationweek.com/mro/aircraft-propulsion/magnetic-expects-cfm56-market-challenges-opportunities-2024
[76] "A320 Base Check Maintenance Inputs," *Aircraft Commerce*, No. 111, 2017. https://www.aircraft-commerce.com/wp-content/uploads/aircraft-commerce-docs/Maintenance/2017/111_MTCE_A.pdf
[77] "12 Aircraft Operating Costs – EUROCONTROL Standard Inputs for Economic Analyses." Retrieved 1 September 2026. https://ansperformance.eu/economics/cba/standard-inputs/v10.0.0/chapters/aircraft_operating_costs.html
[78] Bradley, M. K., and Droney, C. K., "Subsonic Ultra Green Aircraft Research: Phase 2: Hybrid Electric Design Exploration - Volume 2," NF1676L-21005, April 2015.
[79] ocatsaros, "Lithium-Ion Battery Pack Prices Hit Record Low of $139/kWh," BloombergNEF, Nov 26 2023. Retrieved 7 September 2026. https://about.bnef.com/insights/clean-energy/lithium-ion-battery-pack-prices-hit-record-low-of-139-kwh/
[80] "IATA - Fuel Price Monitor." Retrieved 7 September 2026. https://www.iata.org/en/publications/economics/fuel-monitor/
[81] "Minimum Qualification Standards for Oxygen Cyliners Used on Board Aircraft," 2018.
[82] Potsdam, M., Page, M., Liebeck, R., Potsdam, M., Page, M., and Liebeck, R., "Blended Wing Body Analysis and Design," presented at the 15th Applied Aerodynamics Conference, 1997. https://doi.org/10.2514/6.1997-2317
[83] Liebeck, R. H., "Design of the Blended Wing Body Subsonic Transport," *Journal of Aircraft*, Vol. 41, No. 1, 2004, pp. 10–25. https://doi.org/10.2514/1.9084
[84] Drela, M., "Power Balance in Aerodynamic Flows," *AIAA Journal*, Vol. 47, No. 7, 2009, pp. 1761–1771. https://doi.org/10.2514/1.42409